Eur. Phys. J. B (2018) 91: 273
https://doi.org/10.1140/epjb/e2018-90281-7

THE EUROPEAN PHYSICAL JOURNAL B

Regular Article

Magnetic response in silicene, germanene, and stanene rings with ferromagnetic and antiferromagnetic exchange field

Ning Xu[1,a], Jian Wen Ding[2], Bao Lin Wang[3], and Heng Yi Xu[3]

[1] Deparment of Physics, Yancheng Institute of Technology, Yancheng 224051, P.R. China
[2] Deparment of Physics, Xiangtan University, Xiangtan 411105, P.R. China
[3] Departmentof Physics, Nanjing Normal University, Nanjing 210023, P.R. China

Received 24 April 2018 / Received in final form 19 August 2018
Published online 5 November 2018

Abstract. Magnetic response properties of silicene, germanene, and stanene rings have been explored. The total magnetic moment of the rings can be modulated by the exchange field. The magnetic moment of the rings can be regulated and keeps the constant valuewithin certain ferromagnetic exchange filed window. Diamagnetism–paramagnetism or paramagnetism–diamagnetism transitions are observed with the increase of antiferromagnetic exchange field.

1 Introduction

Two-dimensional (2D) material is one of the most active research fields of condense matter physics since the discovery of graphene [1,2]. It has been extended to the group IV 2D materials including silicene, germanene, and stanene [3–15], which are monolayer honeycomb structures of silicon, germanium, and tin, respectively. Silicene was first reported in 2010 and has been grown on different substrate, such as the MoS2 substrate [3], the Ag substrate [4–6], the ZrB2 substrate [7], and the Ir substrate [8]. Germanene is synthesized on the Al substrate [9], the Ge2Pt substrate [10],the Pt substrate [11], and the Au substrate [12,14]. Stanene is synthesized on the Bi2Te3 substrate [15]. Silicene, germanene, and stanene are expected to be two-dimensional time-reversal invariant topological insulators (TIs) [16–18]. TI is a new state of quantum matter that is characterized by an insulating gap in the bulk accompanied with a conducting, linearly dispersed Dirac edge state. Under symmetry-breaking external fields, even more topological phases have been realized [19,20]. More recently, graphene rings (GPRs) have been realized [21,22], by using electron beam lithography technique. The radii of graphene rings range from 200 to 500 nm. Based on tight-binding model, clockwise and counterclockwise persistent currents are observed in armchair quantum rings [22]. The magnetic-field-driven carriers flow clockwise and anticlockwise along the inner and outer edge of rings owing to quantum Hall effect [23]. Similar to that of mesoscopic GPRs, one may anticipate an enhanced magnetic response of silicene, germanene, and stanene ring systems owing to these rich physical properties, such as the strong spin–orbit coupling and adjustable external field.

In the present work, we aim to shed light on the magnetic response mechanism of silicene, germanene, and stanene rings under an applied magnetic field (with the field perpendicular to the plane of the rings). It is shown that these rings possess unusually large diamagnetic moments, which are the result of competition of the spin-up and spin-down electrons. Under ferromagnetic exchange fields, colossal diamagnetic moment is realized and keeps the constant value within certain ferromagnetic exchange filed window. Diamagnetism–paramagnetism or paramagnetism–diamagnetism transitions are observed with the increase of antiferromagnetic exchange field.

2 Model and method

Both silicene, germanene, and stanene can be well described by Kane and Mele's minimal topological insulator model. The Hamiltonian is written as [16,24,25]

$$H_{\mathrm{KM}} = -t \sum_{<i,j>} C_{i\alpha}^{+} C_{j\alpha} + it_0 \sum_{<<i,j>>} v_{ij} C_{i\alpha}^{+} \sigma_{\alpha\beta}^{z} C_{j\beta} \quad (1)$$

where $c_{i\alpha}^{\dagger}(c_{i\alpha})$ is the creation (annihilation) operator for an electron with spin α on site i, and $\langle ij \rangle$ run over all nearest neighbor hopping sites. The first term represents the nearest-neighbor hopping. The second term represents the intrinsic spin–orbit coupling (SOC) involving the next-nearest neighbor hopping with amplitude t_0. $\nu_{ij} = +1(-1)$ if the next-nearest neighbor hopping is anticlockwise (clockwise) with respect to the positive z-axis.

[a] e-mail: xuning79530@126.com

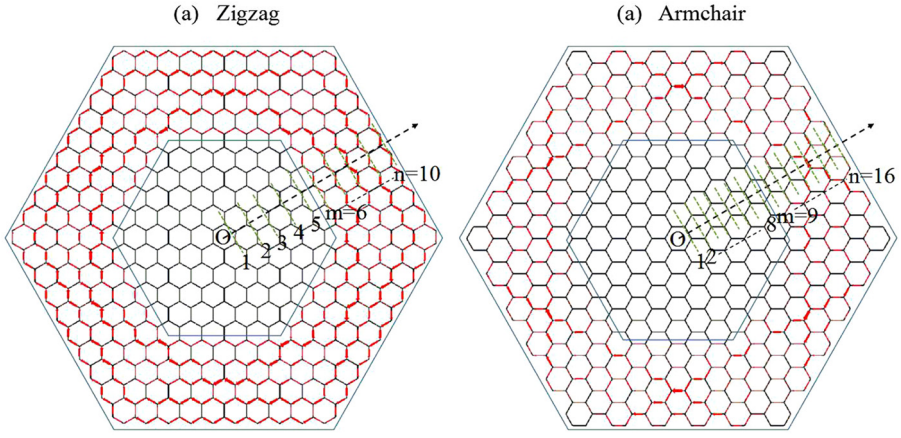

Fig. 1. The schematic illustration of (a) (6, 10) zigzag and (b) (9, 16) armchair ring. The red arrows represent the ring current with their widths proportional to the current strength.

In the following, various perturbation terms are considered. We first consider an out-of-plane antiferromagnetic (OP-AF) exchange field (i.e., the magnetization is perpendicular the plane) [23]

$$H_{\mathrm{AF}} = m_{\mathrm{af}} \sum_{i\alpha\beta} (a^{+}_{i\alpha}\sigma^{Z}_{\alpha\beta}a_{i\beta} - b^{+}_{i\alpha}\sigma^{Z}_{\alpha\beta}b_{i\beta}). \quad (2)$$

Second, we consider an out-of-plane ferromagnetic (OP-FM) exchange field [23].

$$H_{\mathrm{FM}} = m_{\mathrm{fm}} \sum_{i\alpha\beta} c^{+}_{i\alpha}\sigma^{Z}_{\alpha\beta}c_{i\beta}. \quad (3)$$

The latter two terms m_{af} and m_{fm} are exchange fields, which arise from the interaction with a magnetic substrate, where the creation operator $a^{\dagger}_{i\alpha}(b^{\dagger}_{i\alpha})$ acts on sublattice A (B).

The applied magnetic field is perpendicular to the plane of the rings. The effect of the magnetic field enters the Hamiltonian via $H_{ij} = H^{0}_{ij} \exp\left\{i(2\pi/\varphi)\int_{i}^{j} \vec{A}\cdot d\vec{r}\right\}$, where H^{0}_{ij} is the Hamiltonian matrix element for zero field, $\varphi = hc/e$ the flux quantum, and $\vec{A}$ the vector potential [26,27]. The magnetic moment of a silicene ring was calculated in terms of the ring current I in the ring, namely, $M = IS$ where the current element between site i and j is [23,28]

$$I_{ij} = \frac{4e}{\hbar} Im \sum_{n} f(E_n) c^{*}_{in} H_{ij} c_{jn}. \quad (4)$$

Here, $f(E_n)$ being the Fermi factor, c_{in} the eigenvector corresponding to the eigenenergy E_n, and S the area enclosed by the rings.

3 Results and discussions

Figures 1a and 1b are the (6, 10) zigzag and (9, 16) armchair rings, respectively. The inner and outer radii of the rings are labeled by m and n. The induced magnetic moment as a function of magnetic field is shown in Figure 2. In the case of $t_0 = 0.01t$, both the zigzag and armchair rings exhibit diamagnetic response. This is because the persistent current induced by the magnetic field flows clockwise along the rings, as shown in Figure 1, in which the current of any cross section is conserved. The magnetic moments of the zigzag rings decrease linearly with the magnetic field and a jump of the magnetic moment is observed. By analysis of the electronic structure of (6, 13) ring (shown in the inset of Fig. 2a), twofold degenerate energy level is found at the magnetic field $B = 34\,\mathrm{T}$. The spin-up states are shown in black and the spin-down states are shown in red. Thus, the first energy level below the Fermi energy comprise of spin-up and spin-down states, as shown in the inset of Figure 2a. The first energy level consists of spin-down states if $B < 34\,\mathrm{T}$, while the first energy level consists of spin-down states if $B > 34\,\mathrm{T}$. As we all know, the persistent

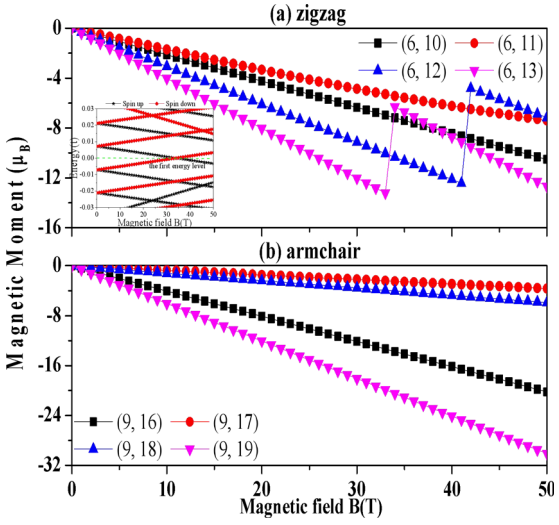

Fig. 2. Magnetic moment as a function of magnetic field strength with the intrinsic SOC for (a) zigzag and (b) armchair ring, respectively.

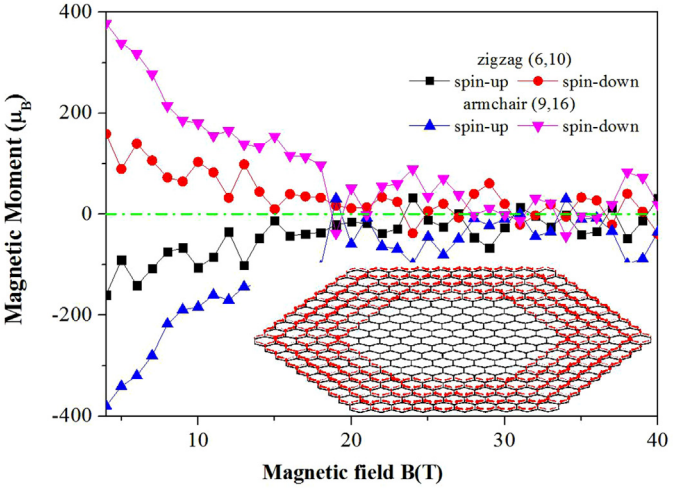

Fig. 3. Magnetic moment of spin-up and spin-down electrons vs. magnetic field strength for (a) zigzag and (b) armchair rings.

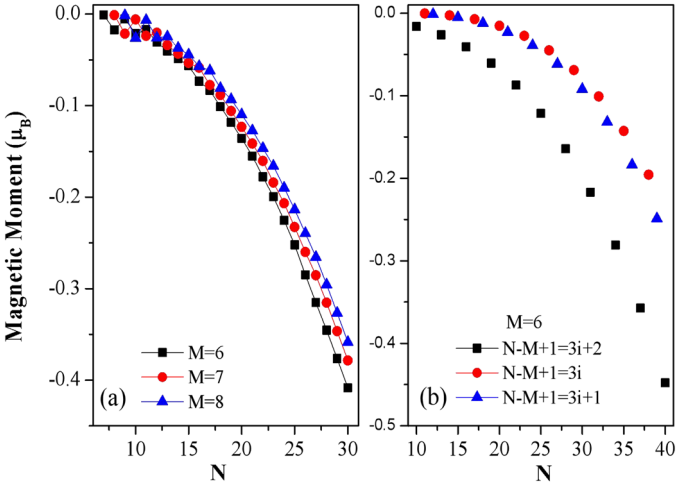

Fig. 4. At the given inner radius, the induced magnetic moment vs. outer radii of (a) zigzag and (b) armchair rings.

current of the mesoscopic rings is mainly decided by electronic structure in accordance to $I_{\rm pc} = -\frac{1}{\Phi 0}\sum_{\rm n}\frac{\partial\varepsilon_n}{\partial\varphi}$ [29,30], where $\varphi = \Phi/\Phi_0$ is the reduced flux with $\Phi_0 = h/e$, ε_n is the eigenlevel of rings. Thus, the spin-down electrons of the first energy level induced by the magnetic field flow anticlockwise along the (6, 13) ring when $B < 34\,\mathrm{T}$. However, the spin-up electrons of the first energy level induced by the magnetic field flow clockwise along the (6, 13) ring, when $B > 34\,\mathrm{T}$. As a result, a jump of the magnetic moment exists at the magnetic field $B = 34$ T. While for the armchair rings, the magnetic moments of the armchair silicene rings decrease linearly with the magnetic field and no jumps are observed. Surprisingly, the magnitude of magnetic moment for (9, 16) and (9, 19) rings are bigger than that of (9, 17) and (9, 18) rings.

The magnetic moment of spin-up and spin-down electrons vs. magnetic field strength is shown in Figure 3. It is shown that in the case of $B = 5\,\mathrm{T}$, the spin-up electrons in zigzag (6, 10) ring flow anticlockwise along the rings and thus the current flow clockwise as shown in the inset of Figure 3, in which colossal diamagnetic moment is observed. The spin-down electrons induced by the magnetic field flow clockwise along the ring and thus the current flow anticlockwise along the ring. Therefore, the total magnetic moment in Figure 2 is the result of competition of spin-up and spin-down electrons. Diamagnetism–paramagnetism or paramagnetism–diamagnetism transitions are observed for that of spin-up and spin-down electrons with the increase of magnetic field.

In Figure 4, the quantum size effect is discussed. At the given inner radius, the absolute value of the magnetic moment for zigzag rings increases exponentially with the increase of outer radius as a whole, as shown in Figure 4a. This is because that with the increase of outer radius, more and more spin-up and spin-down electrons driven by magnetic field flow anticlockwise and clockwise along rings, which forms paramagnetic and diamagnetic

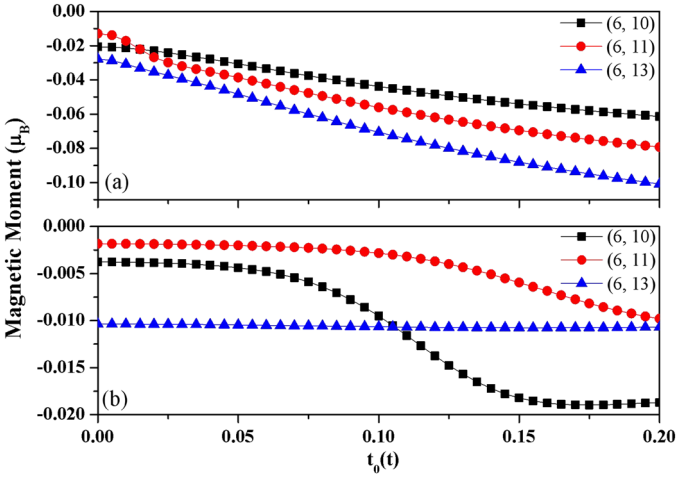

Fig. 5. Induced magnetic moment of (a) zigzag and (b) armchair rings vs. the intrinsic SOC strength at the given magnetic field $B = 0.1\,\mathrm{T}$.

moment. More particularly, the jumps of magnetic moment are observed, when the difference between inner and outer radius is small. The absolute value of the magnetic moment for (6, 8) ring is higher than that of (6, 7) and (6, 9) ring, because of the higher electron group velocity. While for armchair rings, the magnetic moment depends highly on their width. In the case of $t_0 = 0.01t$, the armchair rings are semiconductor. The rings have larger magnetic moment owing to the higher electron group velocity, when the difference between inner and outer radius $N - M + 1 = 3i + 2$ (i is an integer).

In Figure 5a, we find the amplitude of total magnetic moment of zigzag rings decreases exponentially with the intrinsic SOC strength. For armchair rings with $N - M + 1 = 3i + 1$ or $N - M + 1 = 3i + 3$ (i is an integer), the amplitude of total magnetic moment remains almost the same firstly, and then decay exponentially as shown in Figure 5b. While for armchair rings with $N - M + 1 = 3i + 3$, the amplitude of total magnetic

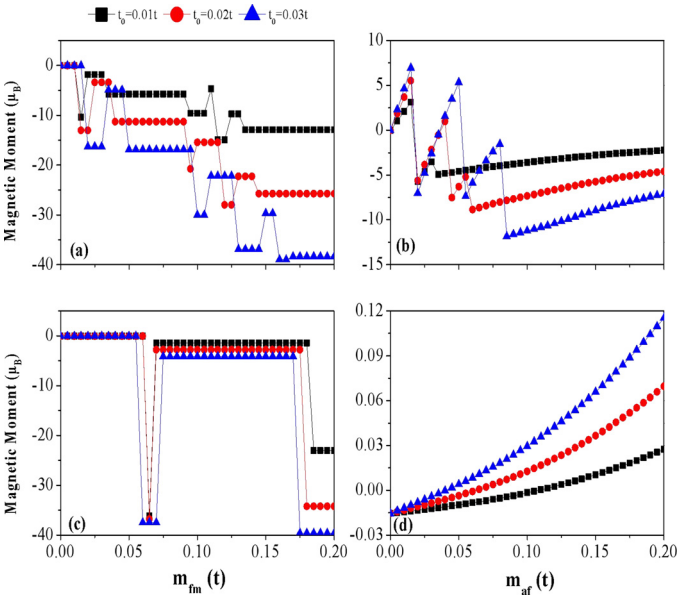

Fig. 6. The induced magnetic moment vs. the strength of the ferromagnetic exchange filed for (a) zigzag (6, 10) and (c) armchair (9, 16) rings. The induced magnetic moment vs. the strength of the antiferromagnetic exchange filed for (b) zigzag (6, 10) and (d) armchair (9, 16) rings.

moment remains almost unchanged. The results mean that the amplitude of total magnetic moment can be adjusted by the intrinsic SOC strength.

In Figure 6, we find that the exchange field m_{fm} has a significant impact on the magnetic moment of the rings. Under the ferromagnetic exchange filed, zigzag and armchair rings remain diamagnetic response. The magnetic moment exhibits step-like oscillation with the increase of the ferromagnetic exchange field and keeps the constant value within certain ferromagnetic exchange filed window. In the presence of the antiferromagnetic exchange filed, paramagnetism–diamagnetism or diamagnetism–paramagnetism transitions are observed in ziagzag rings, and the oscillations of the magnetic moment are observed. While for armchair rings, diamagnetism–paramagnetism transition is observed and the value of magnetic moment increases with the antiferromagnetic exchange filed.

The spin–orbit coupling (SOC) of silicene is to be $t_0 = 3.9$ meV with the hopping parameter $t = 1.6$ eV. The SOC of germanene is about ten times larger than that of silicene, $t_0 = 43$ meV and $t = 1.3$ eV. Recent ab initio calculated results have revealed that $t_0 = 100$ meV and $t = 1.3$ eV in stanene. Figure 7 shows that at a low temperature, the magnetic moment of the silicene, germanene, and stanene rings have a relative weak dependence on the temperature. The value of diamagnetic moment of rings decay exponentially with temperature at high temperature. When the phase coherence length L_ϕ is much larger than L, the system can be described by the eigenfunctions of its Hamiltonian. The temperature induce the electrons around E_F redistribution and temperature suppresses magnetic moment because of the thermal broadening.

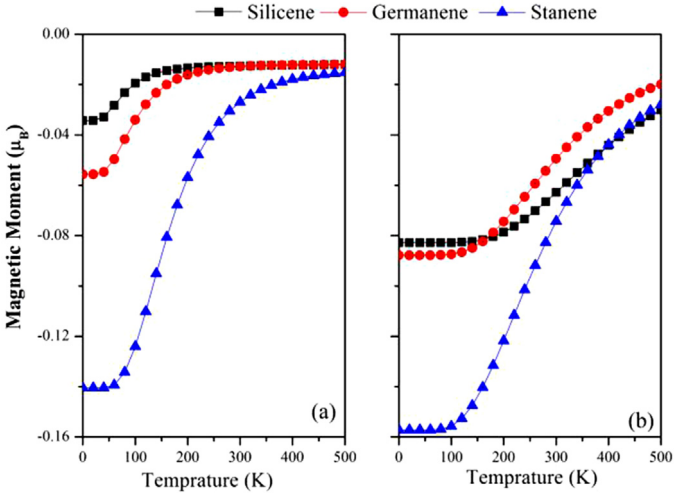

Fig. 7. The induced magnetic moment as a function of temperature of (a) zigzag and (b) armchair rings in a perpendicular magnetic field of 0.2 T.

4 Conclusion

In summary, magnetic response properties of silicene, germanene, and stanene rings have been explored by the tight binding model. Spin-up electrons flow anticlockwise along the rings exhibiting giant orbital paramagnetism, while spin-down electrons flow clockwise along the rings exhibiting giant orbital diamagnetism. Thus, these rings exhibit diamagnetic response, which is the result of competition of spin-up and spin-down electrons. The total magnetic moment can be modulated by the external field. Under ferromagnetic exchange fields, colossal diamagnetic moment is realized and keeps the constant value within certain ferromagnetic exchange filed window. Diamagnetism–paramagnetism or paramagnetism–diamagnetism transitions are observed with the increase of antiferromagnetic exchange field.

This work was supported by the National Natural Science Foundation of China (Grant No.11404278, 11774178).

Author contribution statement

N. Xu and J. W. Ding conceived the research. N. Xu carried out the calculation. N. Xu, J. W. Ding, B. L. Wang and H. Y. Xu analyzed the data. N. Xu wrote the paper.

References

1. K.S. Novoselov, A.K. Geim, S.V. Morozov, D. Jiang, Y. Zhang, S.V. Dubonos, I.V. Grigorieva, A.A. Firsov, Science **306**, 666 (2004)
2. K.S. Novoselov, A.K. Geim, S.V. Morozov, D. Jiang, M. Katsnelson, I.V. Grigorieva, S.V. Dubonos, A.A. Firsov, Nature **438**, 197 (2005)
3. D. Chiappe, E. Scalise, E. Cinquanta, C. Grazianetti, B. van den Broek, M. Fanciulli, M. Houssa, A. Molle, Adv. Mater. **26**, 2096 (2014)

4. P. Vogt, P. De Padova, C. Quaresima, J. Avila, E. Frantzeskakis, M.C. Asensio, A. Resta, B. Ealet, G. Le Lay, Phys. Rev. Lett. **108**, 155501 (2012)
5. C.L. Lin, R. Arafune, K. Kawahara, N. Tsukahara, E. Minamitani, Y. Kim, N. Takagi, M. Kawai, Appl. Phys. Express **5**, 045802 (2012)
6. B. Feng, Z. Ding, S. Meng, Y. Yao, X. He, P. Cheng, L. Chen, K. Wu, Nano Lett. **12**, 3507 (2012)
7. A. Fleurence, R. Friedlein, T. Ozaki, H. Kawai, Y. Wang, Y. Yamada-Takamura, Phys. Rev. Lett. **108**, 245501 (2012)
8. L. Meng, Y. Wang, L. Zhang, S. Du, R. Wu, L. Li, Y. Zhang, G. Li, H. Zhou, W. A. Hofer, H. J. Gao, Nano Lett. **13**, 685 (2013)
9. M. Derivaz, D. Dentel, R. Stephan, M.C. Hxanf, A. Mehdaoui, P. Sonnet, C. Pirri, Nano Lett. **15**, 2510 (2015)
10. P. Bampoulis, L. Zhang, A. Safaei, R. van Gastel, B. Poelsema, H.J.W. Zandvliet, J. Phys.: Condens. Matter **26**, 442001 (2014)
11. L. Li, S. Z. Lu, J. Pan, Z. Qin, Y.Q. Wang, Y. Wang, G.Y. Cao, S. Du, H.J. Gao, Adv. Mater. **26**, 4820 (2014)
12. M. E. Dávila, L. Xian, S. Cahangirov, A. Rubio, G. Le Lay, New J. Phys. **16**, 095002 (2014)
13. F. Zhu, W.J. Chen, Y. Xu, C.L. Gao, D.D. Guan, C. Liu, D. Qian, S.C. Zhang, J.F. Jia, Nat. Mater. **14**, 1020 (2015)
14. J.C. Zhuang, N. Gao, Z. Li, X. Xu, J.O. Wang, J.J. Zhao, S.X. Dou, and Y. Du, ACS Nano **11**, 3553 (2017)
15. J.J. Zhao, H.S. Liu, Z.M. Yu, R. Quhe, S. Zhou, Y. Wang, C.C. Liu, H.X. Zhong, N.N. Han, J. Lu. Y.G. Yao, K.H. Wu, Prog. Mater. Sci. **83**, 24 (2016)
16. C.C. Liu, W. Feng, Y. Yao, Phys. Rev. Lett. **107**, 076802 (2011)
17. C.C. Liu, H. Jiang, Y. Yao, Phys. Rev. Lett. **84**, 195403 (2011)
18. Y. Xu, B. Yan, H.J. Zhang, J. Wang, G. Xu, P. Tang, W. Duan, S.C. Zhang, Phys. Rev. Lett. **111**, 136804 (2011)
19. M. Ezawa, Phys. Rev. Lett. **109**, 055502 (2012)
20. S. Rachel, M. Ezawa, Phys. Rev. B **89**, 195303 (2014)
21. S. Russo, J.B. Oostinga, D. Wehenkel, H.B. Heersche, S.S. Sobhani, L.M.K. Vandersypen, A.F. Morpurgo, Phys. Rev. B **77**, 085413, (2008)
22. D.R. da Costa, A. Chaves, M. Zarenia, J.M. Pereira Jr., G.A. Farias, F.M. Peeters, Phys. Rev. B **89**, 075418 (2014)
23. N. Xu, Q. Chen, H.Y. Tian, J.W. Ding, J.F. Liu, Phys. Lett. A **380**, 3229 (2016)
24. C.L. Kane, E.J. Mele, Phys. Rev. Lett. **95**, 146802 (2005)
25. C.L. Kane, E.J. Mele, Phys. Rev. Lett. **95**, 226801 (2005)
26. M. Graf, P. Vogl, Phys. Rev. B **51**, 4940 (1995)
27. T.B. Boykin, R.C. Bowen, G. Klimeck, Phys. Rev. B **63**, 245314 (2001)
28. N. Xu, Q. Chen, H.Y. Tian, B.L. Wang, J.W. Ding, Phys. Lett. A **380**, 1102 (2016)
29. M.M. Ma, J.W. Ding, N. Xu, Nanoscale **1**, 387 (2009)
30. X. Tang, N. Xu, J.W. Ding, J. Phys.: Condens. Matter **23**, 306002 (2011)